

TECHNICAL REPORT

A Cellular Automaton Model of Electrical Activation in Canine Ventricles: A Validation Study

Prasad B. Gharpure and Christopher R. Johnson

UUSCI-1995-002

Scientific Computing and Imaging Institute
University of Utah
Salt Lake City, UT 84112 USA

1995

Abstract:

An anatomically accurate 3-D cellular automaton model was used for studying electrical propagation in canine ventricles. The heart model geometry was based upon histologically extracted information that takes into account anisotropy of propagation through myocardial fiber orientation. We present results that compare our computer model to experimentally obtained activation sequences from a canine heart. The data generated from the model showed a high correlation, both qualitatively and quantitatively, to experimental results and that the inclusion of the anisotropy of propagation plays an important role when modeling electrical wave propagation. We envision our model as a useful tool in the search for parameters that promote, initiate and sustain ventricular arrhythmia and fibrillation in the heart. Once characterized, these parameters could contribute to determining the arrhythmogenic risk of patients with heart disease.

A Cellular Automaton Model of Electrical Activation in Canine Ventricles: A Validation Study

Prasad B. Gharpure¹ and Christopher R. Johnson²

¹Nora Eccles Harrison Cardiovascular Research and Training Institute and
Department of Bioengineering

²Department of Computer Science
University of Utah

Salt Lake City, Utah 84112

Email: gharpure@vissgi.cvrtri.utah.edu and crj@cs.utah.edu

Abstract

An anatomically accurate 3-D cellular automaton model was used for studying electrical propagation in canine ventricles. The heart model geometry was based upon histologically extracted information that takes into account anisotropy of propagation through myocardial fiber orientation. We present results that compare our computer model to experimentally obtained activation sequences from a canine heart. The data generated from the model showed a high correlation, both qualitatively and quantitatively, to experimental results and that the inclusion of the anisotropy of propagation plays an important role when modeling electrical wave propagation. We envision our model as a useful tool in the search for parameters that promote, initiate and sustain ventricular arrhythmia and fibrillation in the heart. Once characterized, these parameters could contribute to determining the arrhythmogenic risk of patients with heart disease.

Introduction

A heart beat may be summarized as an ordered contraction of the cardiac muscle. Loss of this order decreases the effective functioning of the heart as a pump and results in a reduction of blood outflow. Any deviation from the regular order of cardiac activation is termed a “conduction defect”, and a disturbance of rhythm, resulting from the deviation is termed as an “arrhythmia”, the most extreme, and lethal, form is ventricular fibrillation. Many basic mechanisms of arrhythmia and fibrillation, that are based on some form of self-stimulation or “reentry” of activation, have been proposed

in the literature [1, 2, 3]. However, the ability to predict the likelihood of a particular patient experiencing an episode of arrhythmia or fibrillation is still quite limited. The wave propagation model we describe here was developed to be a step towards investigating the parameters, and their combinations, that promote, initiate and sustain arrhythmia in the heart. Once determined, this set of parameters, which defines an “arrhythmogenic substrate”, would have to be matched to equivalent clinical indices and might then be used to assist in the prediction of arrhythmia in patients.

There exist many models and methods to simulate propagation in heart tissue, however there are currently no models that can accurately simulate propagation, activation, and recovery in the whole heart in a computationally feasible way. All models represent a tradeoff between accuracy and computational limitations defined by the number and complexity of the simulation parameters. Many models utilize membrane current models such as Beeler–Reuter, Ebihara–Johnson, or Luo–Rudy to represent the cellular membrane dynamics. These models represent the cardiac muscle as individual cells coupled to each other by resistive connections between cells [4, 5, 6, 7, 8]. To capture the electrophysiological dynamics with sufficient spatial and temporal fidelity, cellular membrane models must use a finely resolved spatial grid, and simultaneously, need to take small temporal steps. Fine grid resolution means that a large number of elements are required to simulate enough tissue to capture macroscopic events like reentry and arrhythmias. The smaller the temporal steps the more time required to compute the simulations. For example, to model a single membrane patch element using the Ebihara–Johnson model would require about 27 double precision real values, which require 216 bytes to store. To model cardiac tissue with enough resolution to ensure stability and accuracy of the solution, a spatial resolution of 50 microns would be sufficient. Thus a 1 mm cube of heart tissue, equivalent to 1 element in the cellular automaton model, would require $20 \times 20 \times 20 = 8000$ elements which would require $8000 \times 216 = 1,728,000$ bytes or 1.687 Mb of memory.

To capture the physiology and ensure numerical stability, the time step will have to be on the order of microseconds; the resulting amount of data generated per time step would be enormous. Hence it is obvious that the problem, as posed for a 1 mm cube, is large enough to overwhelm most desktop computers. As a result, models based on microscopic scale membrane kinetics have been limited to propagation in 2–D sheets or small 3–D blocks of tissue [4, 9, 8].

Bidomain models, represent heart tissue as two continuous, intertwined spaces, the extracellular and the intracellular, separated from each other all throughout by a thin membrane. The electrical properties of this membrane are modeled using the membrane models mentioned above. Due to the modeling approach, the discretized equations for the bidomain model allow for a spatial and temporal discretization that is coarser than required for the membrane current models without compromising the solution accuracy and stability. The bidomain models have been used to model relatively larger amounts of tissue as compared to the membrane models, but still are primarily restricted to muscle bundles or blocks of tissue. [10, 11, 12, 13, 14].

Some researchers have approached the spread of the activation process mathematically in the

form of a wave propagation problem. In this context, propagation can be modeled using the Huygens principle or more accurately using an eikonal curvature formulation [15], or oblique dipole layer formulations [16, 17, 18, 19, 20].

Propagation may also be modeled as the passing of activation from one element to its neighbors, the whole process governed by preset rules and state parameters. These models are known as cellular automaton models [21, 22, 23, 24, 25, 26]. Using currently available computational means, the wave equation methods and the cellular automata are the only feasible means of simulating propagation in the entire heart. The major goal of this study was to accurately model propagation in the entire heart with a minor requirement that simulations should be completed in a reasonable time on a desktop workstation. Previous studies using cellular automata [27, 28, 23, 25, 26] have been performed on idealized geometries, for example cones or spheroids, or geometries manually digitized from CT or MRI scans, neither of which included measured fiber directions or realistic physiological representations of the activation/recovery phenomena. With the above goals in mind, we developed a cellular automaton model utilizing a real digitized canine heart geometry with measured fiber directions to model the propagation in the heart. Cellular automata are simplistic models of the complex processes, and hence a validation of the results from cellular automation models is imperative. Earlier models, like the model described by Moe *et al.* [21], lacked spatial or temporal information about the model and the parameters that were used. In our model, the spatial and temporal information is inherent as part of the design and hence it is possible to compare our results with experimental studies. In order to validate the results from our model we compared canine experimental data with data obtained from simulations using our model. The results obtained from the comparisons suggest that the cellular automaton models, if based on physiological parameters, can reproduce features that are seen in experimental preparations. The subsequent sections describe the model construction, the heart geometry, the cellular automaton model computational engine. We also describe the studies that were carried out to compare model data with experimental data, and conclude by analyzing our results from the comparison.

Methods

Model Geometry

The geometry we used for our model has been created by Nielsen *et al.* [29] by manually digitizing a canine heart. The geometry is defined in terms of 60 cubic hermite elements constructed from 117 nodes. The nodes are described in a prolate spheroidal coordinate system and in addition to storing information about the spatial locations, they also contain information regarding the local fiber directions. In order to obtain a detailed geometry, the nodes in each of 60 elements need to be interpolated. The basis functions for the interpolations are a combination of linear and cubic hermite polynomials, with the basis functions defined for all the different components that need to be interpolated. Nielsen *et al.* also defined myocardial structures consisting of intertwining parallel branching planes formed by the myocardial fibers, which they termed “myocardial sheets.” The

data describes the sheets in terms of a sheet direction vector, which is a vector lying in the plane of the fibers, orthogonal to the fiber direction. A direction orthogonal to the plane formed by the fiber and sheet vectors is known as the cross sheet vector.

In order to use the geometry for the cellular automation model, we needed to transform the geometry to a cartesian coordinate system and discretize it to a spatial resolution suitable for our simulations. The data obtained from Nielsen *et al.* was interpolated in the prolate spheroidal coordinate system and then each individual point was transformed to the cartesian coordinate system. The transformed points could be completely enclosed within a 100 mm^3 bounding box, and were sampled at a resolution of 1 mm. A 1 mm sampling allowed us to assign integer values to the x, y, and z components of the points, and hence an easy indexing of the element locations in the model. The data set as sampled at 1 mm results in a ventricular geometry represented by 221,329 nodes. Since each node is located on a regular cartesian grid, it has a maximum of 26 first order neighbors. A spatial resolution of 1 mm, when combined with a temporal resolution of 0.1 ms permits us to achieve propagation velocities of up to $1 \text{ mm}/0.1 \text{ ms} = 10 \text{ m/s}$, well beyond that of even the fast elements in the conduction system. In addition, the description of space in terms of millimeters and time in terms of milliseconds, allows us to compare data between the model and animal experiments.

To accurately simulate electrical wave propagation within the heart, based upon experimental observation, the anisotropic nature of cardiac tissue was an important model component [30]. The geometry described above, has data for the fiber, sheet and the cross sheet directions. These three vectors form a local coordinate system, as shown in Figure 1, that is used in our model to calculate the local propagation velocities from each element to its neighbors.

The process of interpolation, sampling the geometry to obtain the locations and the fiber, sheet and cross sheet vectors is a one time process. The sampled geometry is stored in a file to be reused for all simulations.

Cellular Automaton Model

A cellular automaton is defined by states of the elements and the rules that govern the transition from one state to the next. We now describe the states, rules and the parameters that we used to model activation, recovery and propagation in our model.

All of the elements that constitute the ventricular geometry are modeled to behave as a cubic block of tissue with the cellular properties remaining constant across the individual block. The basic rules for our model are an extension of the 2-D cellular automaton model first described by Moe *et al.* [21] and extensively used by Abildskov [31, 32, 33].

A simulated action potential, which is equivalent to the state diagram, for the model is shown in Figure 2. The first state we encounter is labeled 5*, and is the resting state. An element in this state can be excited by an external stimulus or by an activated neighbor. On a subsequent

*The numbering of the states is arbitrary, and is defined as in the model described by Moe *et al.* [21]

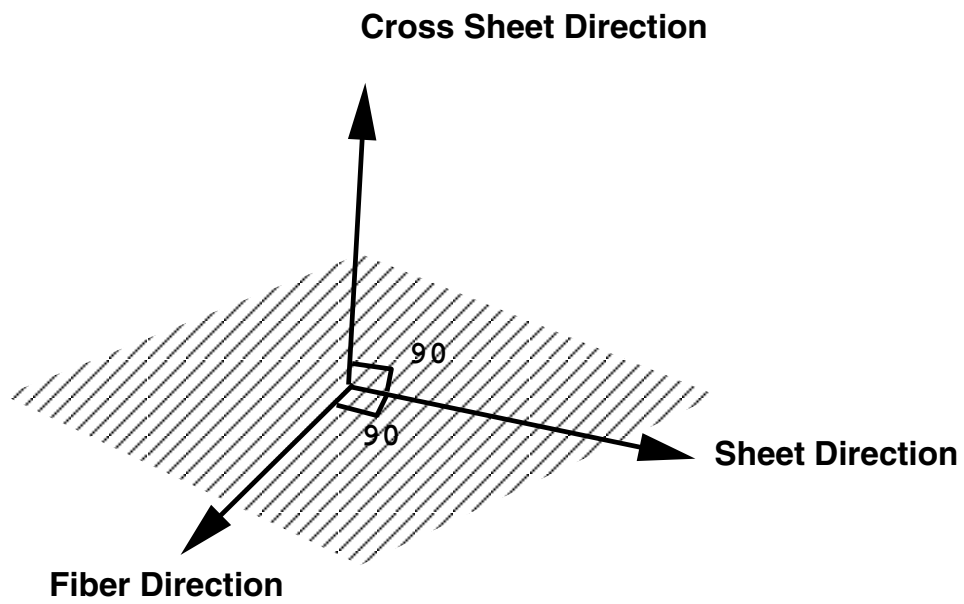


Figure 1: Model representations of fiber, sheet and cross sheet directions

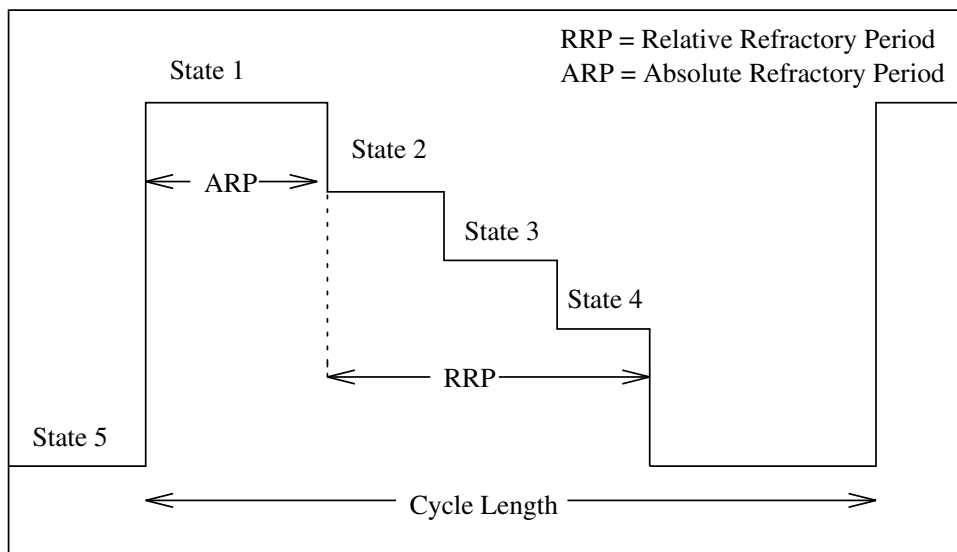


Figure 2: A simulated action potential showing the different states 1–5

time step, the element changes from state 5 to state 1, the first activation, or absolute refractory state, in which no subsequent activation is possible. As a continuation of this activation process, each activated element propagates the activation to all 26 of its nearest neighbors. State 1 is the absolutely refractory state. In this state the element may not be activated either by an external stimulus or by an activated neighbor. The duration of the absolute refractory state, the absolutely refractory period (*ARP*), is not constant but is proportional to the square root of the previous cycle length (*CL*) [21] according to.

$$ARP = \sqrt{K \times CL} \quad (1)$$

The constant of proportionality K , determines the recovery properties of the element. Elements with smaller K values recover faster than elements with a larger K value. Since the parameter K determines recovery, it may be considered to represent the effects of the recovery currents. The element, after completing the duration of the absolutely refractory state enters state 2, the first of the three relatively refractory states 2–4. In these states the element may be excited by an external stimulus, but the response to the activation is preceded by a delay. This delay progressively decreases as the element becomes more recovered. Associating a conduction delay to the degree of recovery allows us to simulate slow propagation in partially recovered myocardium. The durations of states 2–4 are fixed for each simulation and independent of any other parameter. The cycle length (*CL*), for an element, is defined as the duration from the onset of one activation to the onset of the next.

From the definition of refractory time, it can be observed that *CL* values from a previous cycle length are required for the calculation of the *ARP* even for the first beat. A further analysis of the interplay between K and *CL* reveals the following relationship:

$$CL = ARP + RRP + T \quad (2)$$

where *RRP* is the Relative Refractory period and T is the time to the next stimulus. If the stimulus frequency is increased, it is seen that the shortest attainable cycle length is then

$$CL = ARP + D1 \quad (3)$$

where $D1$ is the delay for propagation into a cell in state 2. Substituting (3) into equation (1) and squaring both sides yields

$$ARP^2 = K \times (ARP + D1) \quad (4)$$

upon solving for *ARP*, we obtain,

$$ARP = \frac{K \pm \sqrt{K^2 + 4 \times K \times D1}}{2} \quad (5)$$

The negative root of equation (5) can be ignored as its solutions leads to the unphysiological situation of $ARP \leq 0$. However, the positive root of equation (5) shows that for the shortest cycle length, or the maximal firing frequency, the *ARP* is totally dependant on K and independent of the previous cycle length. K thus determines the duration of the shortest cycle length, that can be

achieved by the element and gives us the means to calculate K from experimental studies on tissue groups or individual cells.

The model is designed in such a way that K and CL values may be assigned individually and thus randomly within a given minimum and maximum value. This individual assignment of the two principal parameters that determine recovery allow us to incorporate inhomogeneity of recovery in the model. Previous studies have shown a strong link between the spatial heterogeneity of repolarization characteristics and susceptibility to ventricular fibrillation [32, 33, 31]. Individual parameter setting also allows model parameters to be set on the basis of tissue type assignments. This permits us to mimic the experimental finding that epicardial tissue recovers faster than endocardial [34] by adjusting the mean value of K in both regions

To model cardiac electrical activity, the model must mimic propagation in the heart, which moves from cell to cell via low resistance gap junctions in the intercalated disks at cell interfaces. The continuance of the spread of the activation from one cell to the next manifests macroscopically as a propagating activation wavefront. Impulse propagation in the model mimics the electrophysiology by allowing each cell to excite its (excitable) first-order neighbors. Propagation velocity is a model parameter set to different physiological values in each of the fiber, sheet, and cross-sheet directions. An average velocity to each neighbor is calculated by constructing an ellipsoid using the three principal velocities and using the magnitude of the vector in the direction of the neighbor that intersects the boundary of the ellipsoid. From the average velocity of these three component amplitudes, along with the direction to each neighbor relative to the local fiber orientation, a time delay, to all the neighbors, is computed for each cell in the model. This delay calculation is a simple velocity and distance equation that yields time. The time delay is saved in terms of time steps needed for activation to leave that cell and travel to its first order neighbor. Since the fiber directions and the propagation velocities are assumed to be constant throughout the duration of the simulation, these delays are calculated once at the beginning of the simulation.

Propagation delay also depends on the state of the neighboring cells. If a neighbor is in state 5, then the delay in propagation is negligible (one time step), but if the neighbor is in the absolute refractory state, it is not excited at all. For neighbors in any of the relative refractory states, an additional delay, proportional to the state of the cell, is added to that calculated from the propagation velocity. The delay, proportional to the state of the target cell, is a user specified value. To illustrate the process, consider a propagation velocity of 1 m/s along the fiber direction and a neighbor in state 5, 1 mm away from the element lying along the fiber direction. The velocity of propagation to the neighbor is 1 m/s, so the delay would be 1 ms or 10 time steps. The cell being excited is in state 5 so that the total delay would be $10 + 1 = 11$ time steps. If the neighbor were in state 2, the delay would be $10 + \text{delay_state_2}$ time steps.

A potential conflict arises when, as shown in figure 3, an element receives activations from different directions. The element in the bottom right activates first and schedules the element on top to fire 30 ms later. The element at the bottom left fires 2 ms later and schedules the element at the top to fire 10 ms after that. The model resolves this by allowing the target element at the

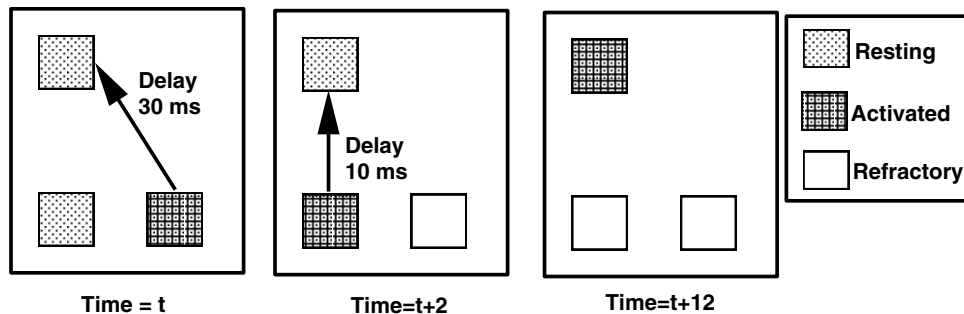


Figure 3: Activation shown propagating along the fastest available path

top to respond to the second activation and then blocks the first activation. By this mechanism, propagation will always proceed along the fastest available path.

The model, as described so far, has facilities for impulse propagation but contains no inherent activation. Activation occurs through the presence of stimulus/pacing sites. A pacing site is conceived to act as an external stimulating electrode, as used in canine experiments and has the following properties: a pacing site may be situated at any element location in the model and a pacing site is configured to fire at a specified time, for a specified duration, and at a specified frequency. An active stimulus site will excite an adjacent element only if the element is not in the absolute refractory state. Stimulus sites may be set anywhere in the model and more than one site, with different firing characteristics, may share the same location. The current implementation of our cellular automaton model does not contain an explicit conduction system, however stimulus sites may be set at specific locations and scheduled to fire sequentially in a manner that imitates the conduction system. A separate MOTIF based 3-D graphical program, as shown in Figure 4, has been implemented to facilitate the specification of the stimulus sites.

In animal experiments and simulations on 2-D tissue preparations, re-entrant circuits have been shown to anchor to regions of inexcitability, such as dead tissue, scar tissue or blood vessels. In addition, inexcitable tissue forms a barrier to the propagating wavefront and helps to increase “fragmentation” of the wavefront, thus promote fibrillation. The characterization of fibrillation is one of the future goals of our model, hence the model was designed to incorporate inexcitable regions. The locations of such “dead cells” may be specified with the same 3-D MOTIF program (see Figure 4). Any anatomical region of the heart model where the user wishes to simulate dead tissue (conduction block) may be marked using the above mentioned program. The dead cell locations are saved to a file and may be reused for later simulations.

Although the model allows us to distribute values of K and CL randomly throughout the volume, in the real heart there is a component of variability of recovery that is bound to the anatomy. The epicardium has cells with shorter cycle lengths as compared to cells on the endocardium. In order to simulate this distribution, the geometry was classified into 10 regions based on the anatomy of the ventricles. The classification is described in Table 1. Minimum and maximum initial cycle

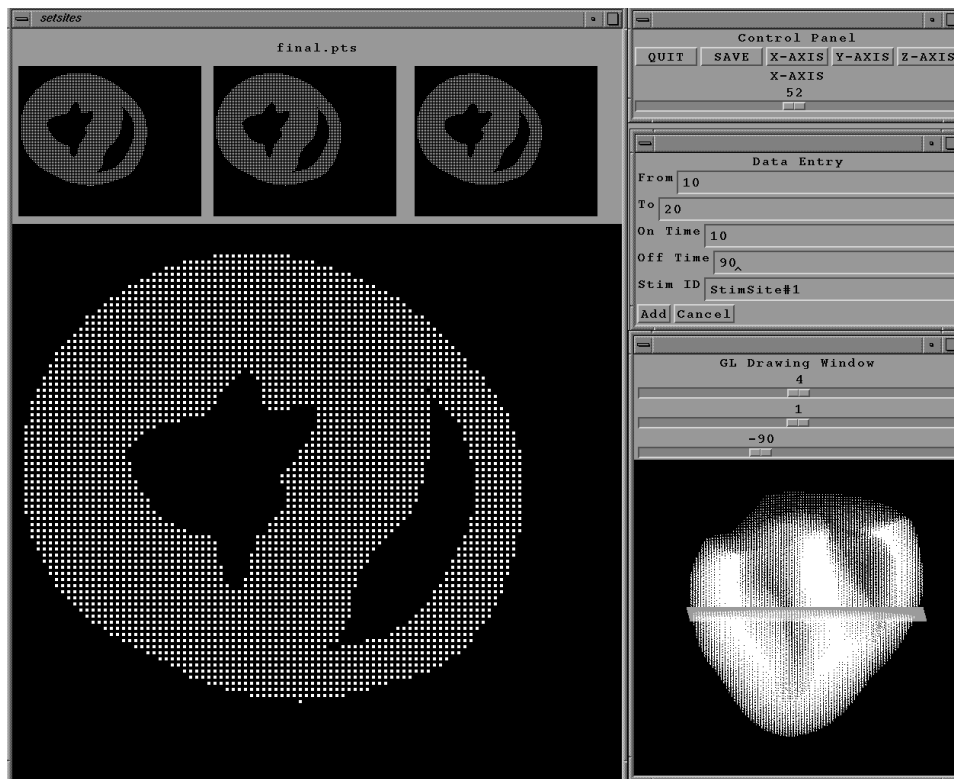


Figure 4: Graphical User Interface for Stimulus Sites and Dead Cells

Region Number	Region Name	Classification Method
1	Epicardium	Outermost layer of Elements
2	Sub Epicardium 1	Immediate neighbors of Region 1
3	Sub Epicardium 2	Immediate neighbors of Region 2
4	LV Endocardium	Innermost layer of the left ventricle
5	LV Sub Endocardium 1	Immediate neighbors of Region 4
6	LV Sub Endocardium 2	Immediate neighbors of Region 5
7	RV Endocardium	Innermost layer of the right ventricle
8	RV Sub Endocardium 1	Immediate neighbors of Region 7
9	RV Sub Endocardium 2	Immediate neighbors of Region 8
10	Rest	Elements that do not fall in any of the above categories

Table 1: Characterization of the different tissue types within the model.

lengths and K values may be specified for any of the tissue types mentioned above. In addition, the classification may be used as a visual aid. The propagation in any of the 10 tissue types may be visualized independently which allows us to observe any changes in wavefront shape as it moves from the epicardium to the endocardium.

Most of the input for the simulation, such as the location of the geometry file, the principal velocities, minimum and maximum K , minimum and maximum CL etc., come from the simulation parameter file. The output of the simulation describes the states of all the elements in the simulation, sampled at regular intervals (typically 1 ms = 10 time steps). The program also records the time of the first activation for all the elements during the course of the simulation, from which isochrone information may be obtained.

Post processing of the datafile includes visualization, isochrone extraction and electrogram calculation. Data from the simulation can be visualized using a MOTIF and SGI GL based 3-D display program (see Figure 5). Each element in the model is assigned a color based on its state. The program allows us to step temporally through the entire dataset, animating the propagation wavefront. In addition, the dataset may be rotated around any of the 3 principal axes, or slices of the data may be visualized individually. Using the tissue type characterization the data for a particular anatomic surface may also be viewed individually. A fast and interactive 3-D volume rendering algorithm, called differential volume rendering, has also been devised to display the activation wavefront as an opaque surface, propagating through a semi-transparent myocardium [35, 36]. Activation isochrones may be extracted for the entire dataset or only from certain selected regions and then utilized for visual or statistical correlation with experimental data. Isochrones can be visualized using Map3D [37], or other visualization systems like AVS, SGI Iris Explorer or IBM Data Explorer that provide automatic isosurface extraction. Electrograms may be calculated from the dataset by assigning electrical potential values to the individual states. We used a finite difference method to compute the potential dipoles for every element. The dot product of the dipoles with the distance vector to the location of the simulated recording electrode were then summed over the entire heart [38, 31, 32, 33, 26]. Multiple site electrograms may be displayed using Map3D as isopotential maps.

The model was implemented in the ‘C’ programming language and all the simulations were performed on an SGI Indigo running IRIX and on an IBM-RS6000 running AIX. The visualization tools were implemented in C++ using X-Windows, MOTIF, and mixed mode GL programming on an SGI Indigo.

Experimental Studies and Model Comparison

The cellular automaton model uses a simple set of rules to represent the complex physiological processes that result in electrical impulse generation, conduction and propagation. The simplicity of the assumptions allows one to simulate wave propagation within a realistic whole heart model, however, this simplicity inevitably results in some loss of accuracy. In order to quantify the limitations of the model and hence assess its usefulness, comparison studies with experimental results

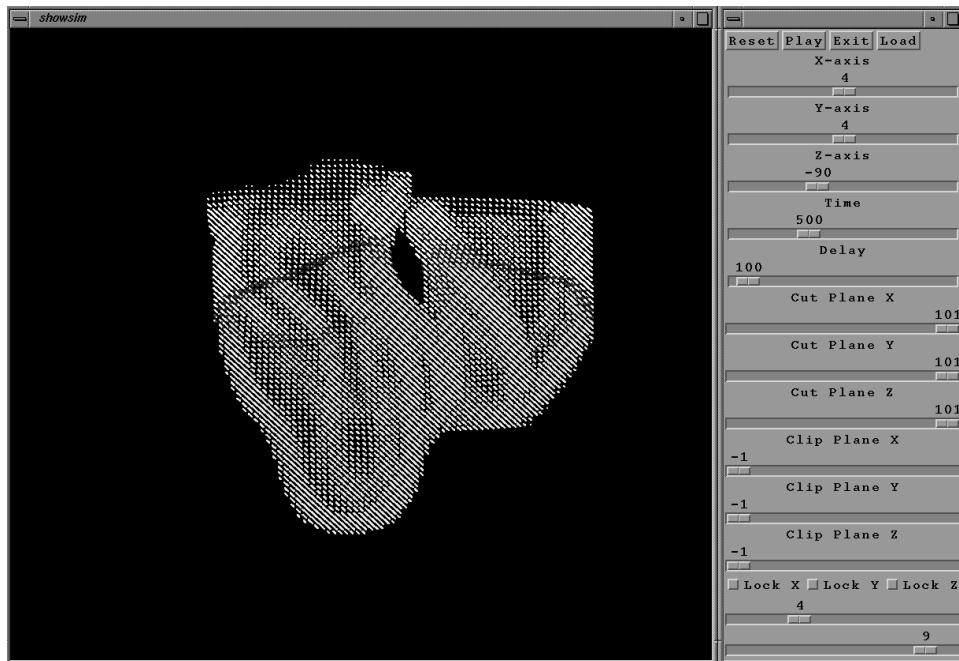


Figure 5: Visualizing Activation in the Right and Left Ventricular Endocardia.

were performed. These studies consisted of comparing activation isochrones obtained from canine experiments with simulation results from the model, under the same or similar stimulus parameters.

The experimental data were obtained from canine experiments performed by Dr. B. Taccardi at the Cardiovascular Research and Training Institute (CVRTI). To prepare the measurement electrodes, a thin extensible nylon stocking was slipped over a plaster model of a dogs heart and 242 silver wires 3 mils in diameter were attached to the sock in positions corresponding to positions earlier marked on the plaster model. The wires were fully insulated except for the last 2–3 mm and the exposed end was secured to the stocking with a tiny knot 0.15 mm in diameter. Excess uninsulated wire was then removed and anatomical landmarks were traced on the sock. In the experiment, the sock was placed on the epicardial surface of a dog heart that had been surgically exposed and suspended in a pericardial cradle, under pentobarbital anesthesia (30 mg/Kg). A similar protocol has been followed in other experiments described by Taccardi [39, 40]. Unipolar electrographic signals from 242 sock electrodes were simultaneously amplified, sampled at 1 KHz per channel, digitized (12 bits) and stored in a MicroVax II disk memory. The heart was sequentially paced from 45 sites selected out of the 242 electrodes the pacing sites covering the entire epicardium. During the pacing, electrographic recordings were made from the remaining 241 electrodes and the data for the pacing electrode were reconstructed from the neighboring electrodes. Activation isochrones were then extracted from the recorded data by determining the time of most rapid downward deflection in each electrogram.

The geometry of the epicardial sock along with the electrodes was first digitized manually and

then scaled and translated to match the dimensions of the model heart using an affine transformation that did not warp the geometry in any manner. The transformation was performed by finding the x, y and z extrema in the two geometries and applying appropriate scaling factors to match the extrema. A translation was also required since the two geometries were not digitized using the same origin. Since the scaling was affine, the values of the three principal velocities that were obtained from the experiment would not be expected to be correct in an absolute sense, but their basic ratios would be maintained. Pacing site locations on the model geometry were then obtained from the electrode locations in the transformed heart geometry. Due to minor differences in the geometry, not all the electrode locations transformed to epicardial locations on the model. In such cases, the nearest epicardial point in the model was selected to be a pacing site.

A total of 45 different simulations were carried out using propagation velocity values of 1 m/s along the fiber direction, 0.33 m/s along the sheet direction and 0.2 m/s along the cross sheet direction. These values were arbitrarily selected as a first guess for the optimization process described later. Each simulation was run for a duration of 100 ms (1000 time steps). The isochrone data were extracted for the 242 nodes corresponding to the measurement sites. Isochrones from the simulation were then displayed alongside the experimental isochrones using Map3D and visually compared. The best correlating site, as decided by visual inspection, was chosen and an optimization process to obtain the propagation velocities that increased correlation and minimized the relative error between the simulated and experimental data sets was performed. The optimization process used a brute force approach consisting of stepping through a range of values for the velocities, comparing the resulting simulations with experimental data, and observing the relative error, variance and correlation coefficient. The process was completed when the values for all the three velocities minimized the error and maximized the correlation coefficient. Using the values obtained from the optimization, the simulations were rerun and variance, correlation coefficients, relative error for all the 45 sites were calculated. The comparisons were limited to the first 50 ms of the activation sequence to prevent effects of the conduction system from obscuring the local activation comparisons. Also the electrode that was used for pacing was ignored in the error analysis. The focus was on comparing activation wavefronts; recovery properties of the model were not considered. All of the simulations were performed under homogeneous distribution of the recovery properties. The results obtained from the comparisons with anisotropic simulations are presented below.

Results and Discussion

The model was designed to run efficiently on available resources. Typical simulations running for 5000 time steps (500 ms) require 18–20 megabytes of memory and create datafiles that are 5–9 megabytes in size. The total duration of the simulation of 5000 time steps is 7–8 minutes. Thus simulations of whole heart electrical wave propagation are feasible even on the single desktop platforms mentioned above.

Comparisons between simulations and experiment

Initially some of the simulations were performed under isotropic conditions using velocities of 1.0 m/s for the fiber, sheet and cross sheet directions. These simulations were quickly discarded because the activation isochrones did not visually compare with the experimental data. An example of an isotropic simulation is shown in Figure 6. One can see that the isochrones do not visually compare well and the quantitative estimates of the variance, relative error, and correlation coefficients, as compared to the corresponding anisotropic simulation shown in Figure 7 are also poor. Further simulations with isotropic propagation were not performed and the subsequent paragraphs discuss only the data obtained from the anisotropic simulations.

Visual comparison of the isochrone maps for both simulated and experimental data revealed many similarities in spite of the fact that the hearts were from different animals, the geometries were scaled to match approximately and also the experimental data was subject to recording and interpolation errors. The velocities used for the fiber, sheet and cross sheet directions were obtained from the optimization process and are specific to this particular experimental preparation. The velocity along fiber direction was 1.09 m/s, along the sheet direction was 0.45 m/s and along the cross sheet direction was 0.3 m/s, representing a fiber velocity that was 2.4 times faster than the sheet velocity and 3.6 times faster than the cross sheet velocities. Isochrone plots obtained from the simulations were compared with similar plots from experiments both visually and statistically in terms of variance, relative error and correlation coefficient analysis. The relative error applied to data from stimulation at all 45 sites ranged from 0.179 to 0.438 with a mean of 0.284 and a standard deviation of 0.0873, and the correlation coefficients ranged from 0.927 to 0.990. These values appeared to agree well with the results of visual comparisons. However some of the visual comparisons were biased by the fact that in the experimental data set, an incorrect reconstruction of the potential at the site of activation caused an apparent shift of the activation focus to one of the neighbors. This is the main reason why we ignored data from the activation site in our error analysis. It can be seen from Figures 7–14 that the isochrone patterns from experimental and simulated data are very similar and only begin to diverge at the same time that remote breakthrough sites start appearing. Due to the absence of a conduction system in the model, only data within the first 50 ms is valid. The tables below each figure display the variance, relative error and correlation coefficients for activation times from stimulation at that site.

Figures 15 and 16 show examples of the least similarity between the model and experimental data sets. Most of the poor correlations were obtained from electrode sites on the right ventricular epicardium, which may, at least in part, be due to the fact that the right ventricular wall is much thinner than the left and the fibers rotate as much as 90–120 degrees across the wall. The right ventricular wall thickness in the model is only 8–10 elements and the wavefront may not be able to curve fast enough in space to follow this rapid change in fiber orientation.

Figure 14 represents one of the best matches that were obtained from the comparison. The data from this stimulation site, situated superiorly on the free wall of the left ventricle, has the highest correlation coefficient and visual inspection also shows a good match, especially in the

early isochrones. However, in the later isochrones an epicardial breakthrough, presumably due to Purkinje system conduction, appears in the experimental preparations and further comparisons degrade rapidly. Another striking similarity between the model and the experimental data set is the agreement in the increase in wavefront speed as seen on the right side of both images. This is probably an effect of anisotropy of conduction due to the fiber directions. We would expect some difference in the exact location of the speedup due to the fact that the experimental and model hearts are from different animals and variations in the fiber directions would be expected.

Figure 8 represents the case where the relative error was the smallest of all the simulations. The small relative error may be linked to the concomitant absence of early epicardial breakthroughs in the experimental potentials. The relative loss of correlation is due to the previously mentioned incorrect reconstruction of the potentials at the stimulus site, in the experimental data. This error causes an apparent shift in the central location of the concentric isochrones, and hence the loss of correlation. Also seen here is the speedup towards the left, as the propagation proceeds towards the apex. It is significantly faster in the experimental data than the simulated data and may be due to propagation through the conduction system.

Figure 15 shows data with the lowest correlation and a high relative error. In fact, the visual correlation of the two sets also shows major differences. This large difference can be linked to the presence of multiple, in this case at least three, breakthrough sites seen in the experimental data set. The presence of the multiple breakthrough sites indicates a strong component of activation carried by the conduction system, making comparison with the model difficult. The second reason for the observed differences might be related to the anatomical location of the site, which is on the free wall of the right ventricle. As explained earlier the number of elements that are available to carry the fiber rotation through the right ventricular free wall is about 8–12 and thus the transmural rotation is probably not captured correctly in the simulation.

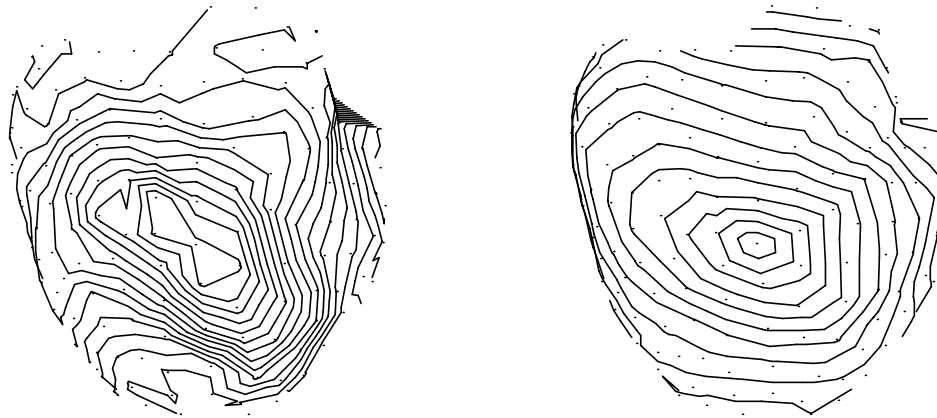
Conclusions

Our research goal was to develop an anatomically accurate 3-D model to simulate anisotropic electrical propagation in the ventricles of the heart. In addition we wanted our model to be easy to use, interactive, and run on a desktop workstation. The model satisfies all the above computational goals. The poor agreement achieved using isotropic simulations from the model and the results obtained from the anisotropic simulations clearly show that anisotropy of propagation is extremely important in determining the shape and directions of the activation wavefront. High correlations and low errors obtained from the comparisons serve to strengthen our belief that the model is capable of simulating the propagation of activation in the ventricles. Cellular automata models can be valuable tools to assist in studying the complex process of propagation in the heart. One limitation of the model is its lack of a conduction system which prevents us from simulating beyond the first 50 ms. The lack of atria in the model does not weaken its utility, since conduction abnormalities in the atria, though serious, are not life threatening immediately. On the other hand,



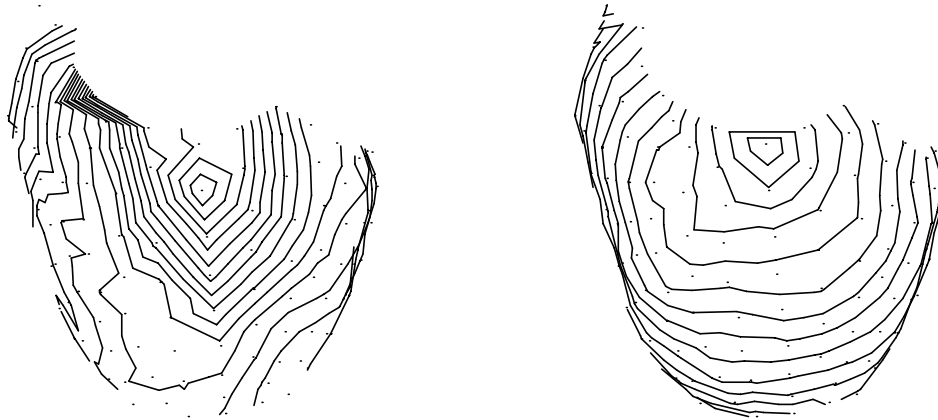
Experimental		Simulated
Variance	Relative Error	Correlation Coeff.
15.43618	0.44405	0.89622

Figure 6: Isochrones from Site #2 under Isotropic conditions



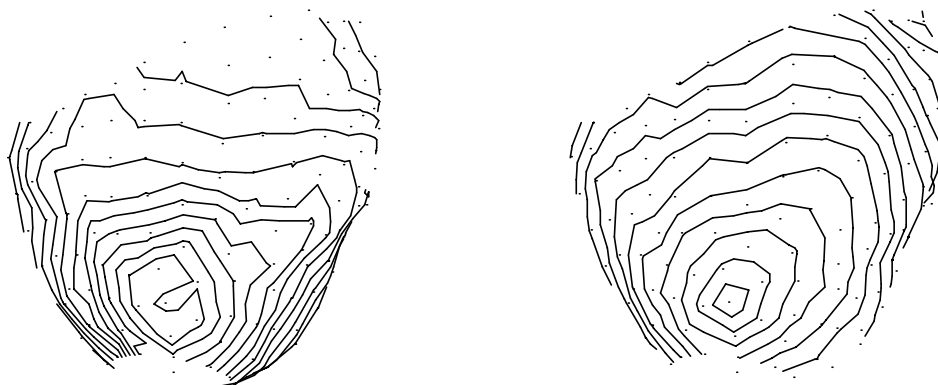
Experimental		Simulated
Variance	Relative Error	Correlation Coeff.
7.69531	0.23437	0.98209

Figure 7: Isochrones from Site #2



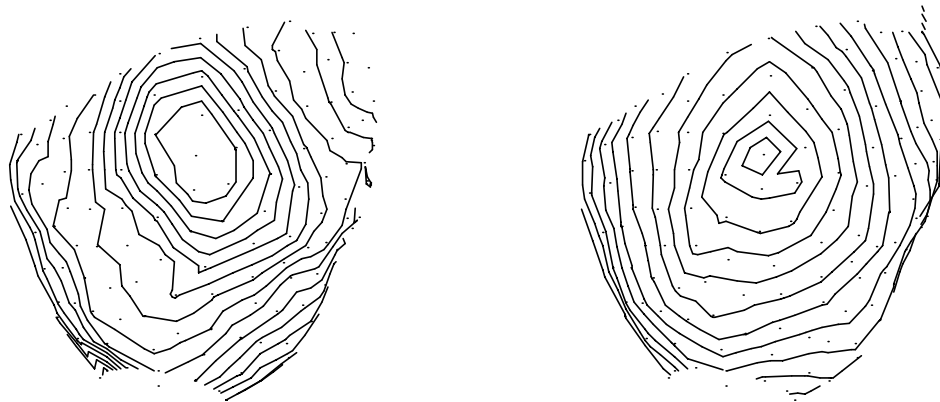
Experimental		Simulated
Variance	Relative Error	Correlation Coeff.
6.41953	0.17113	0.98566

Figure 8: Isochrones from site #16



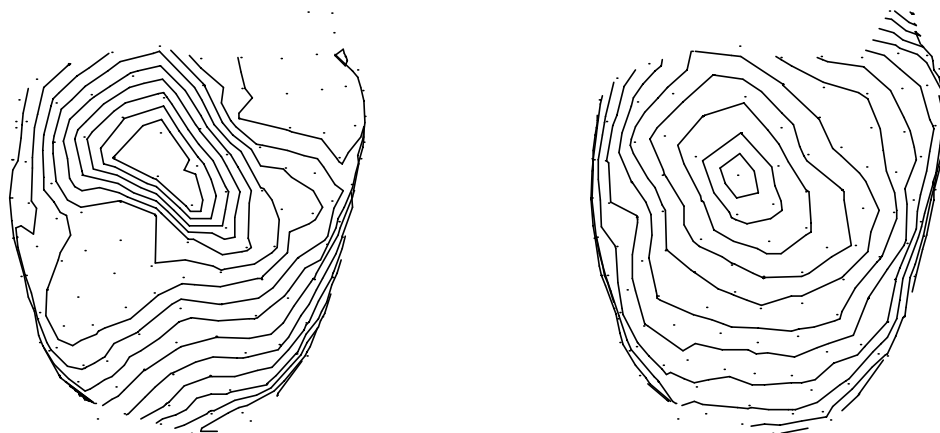
Experimental		Simulated
Variance	Relative Error	Correlation Coeff.
10.16701	0.36873	0.98667

Figure 9: Isochrones from site #31



Experimental		Simulated
Variance	Relative Error	Correlation Coeff.
7.61587	0.22966	0.98018

Figure 10: Isochrones from site #36



Experimental		Simulated
Variance	Relative Error	Correlation Coeff.
8.32111	0.25519	0.98092

Figure 11: Isochrones from site #39

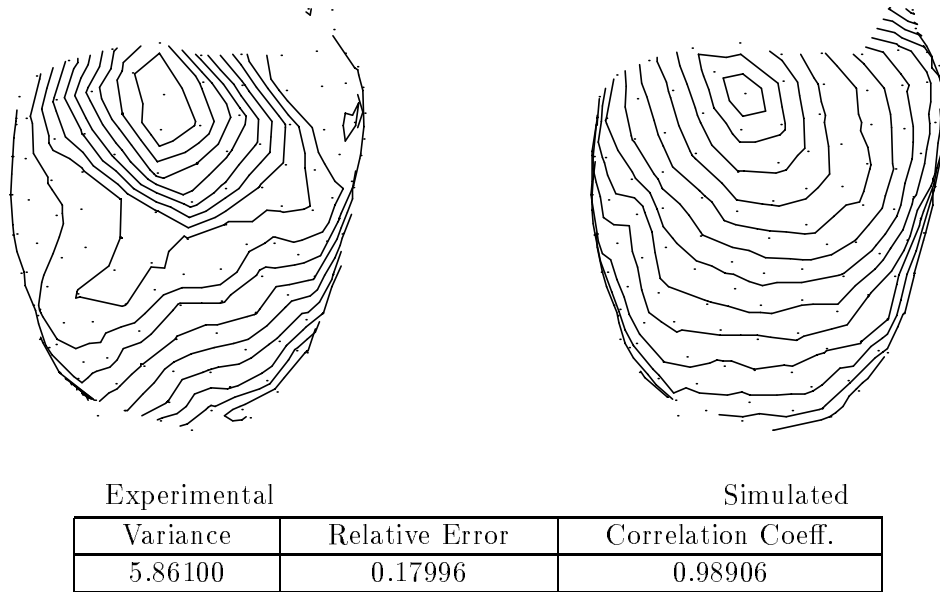


Figure 12: Isochrones from site #40

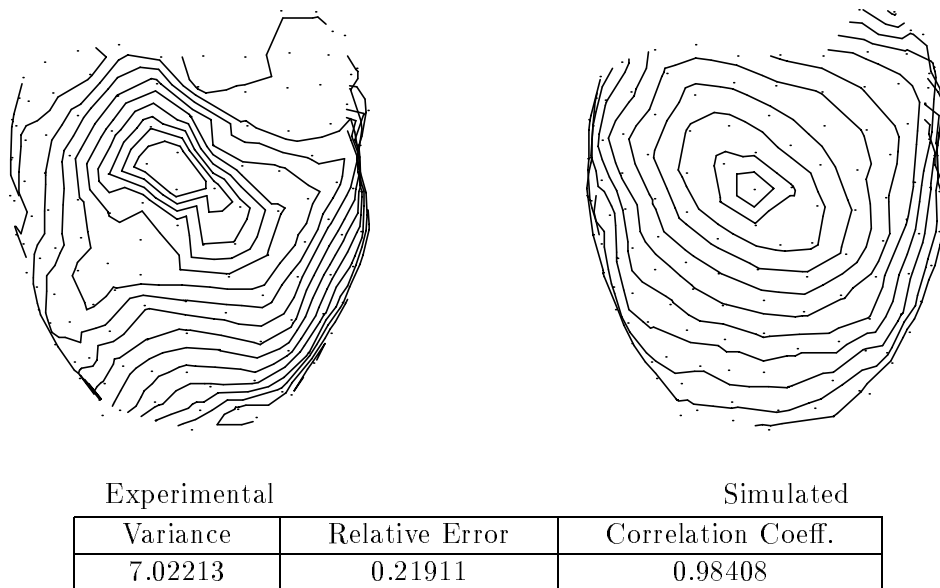
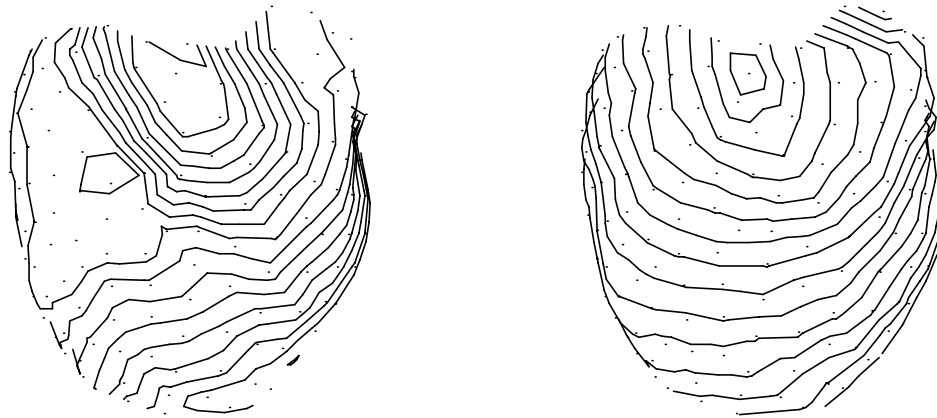
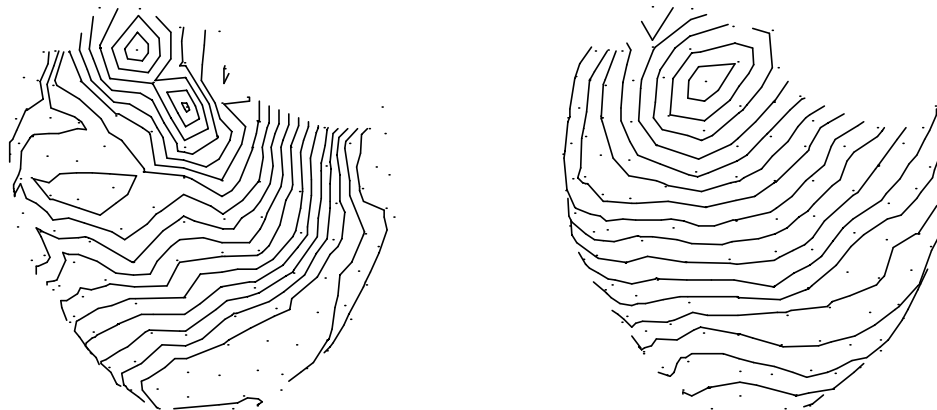


Figure 13: Isochrones from site #43



Experimental		Simulated
Variance	Relative Error	Correlation Coeff.
5.60864	0.18550	0.99006

Figure 14: Isochrones from site #44



Experimental		Simulated
Variance	Relative Error	Correlation Coeff.
12.81529	0.38592	0.92779

Figure 15: Isochrones from site #5

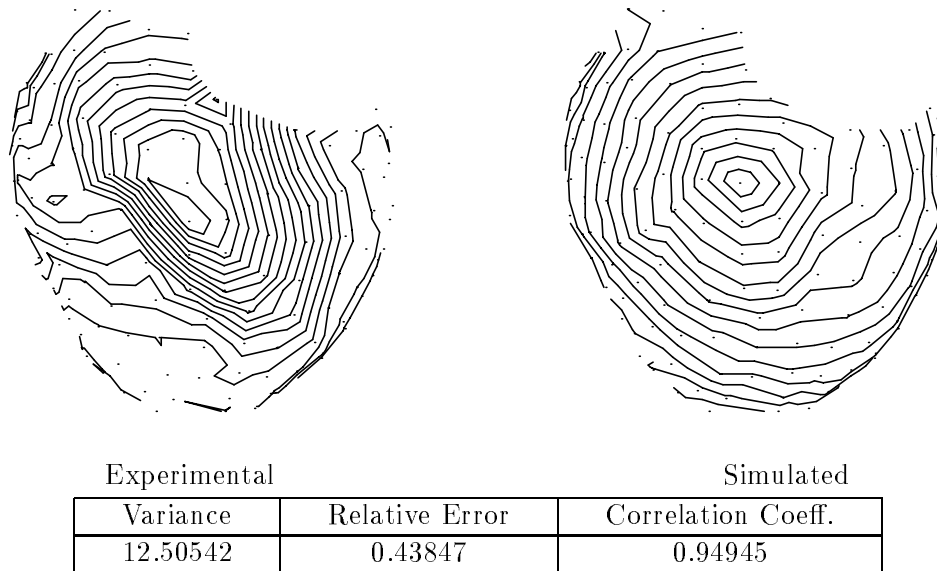


Figure 16: Isochrones from site #8

conduction abnormalities in the ventricles demand immediate treatment, or else death results. The loss of the atria can be made up by faster pacing sites setup near the septum close to the A–V node. An additional weakness of the model is its inability to accurately capture the fiber rotations in the right ventricle. However this is an implementation dependent problem and models constructed on a finer grid would probably be able to capture the fiber rotation more accurately. The finer resolved model would achieve more accuracy, esp. in the right ventricle, but due to the cellular automaton approach that we used, extra elements, would be added to the left ventricular walls and septum, without significantly increasing the accuracy in these regions. These extra elements would make the simulations computationally more demanding with respect to the memory and time required for the simulations. A strength of the modeling approach is that the data may be visualized in ways that are impossible to implement in an experimental setup. In the future, we plan to carry out studies to explore the factors, particularly the distributions of recovery properties and cycle lengths, that promote fibrillation and to determine whether anisotropy has a protective or detrimental effect with respect to the vulnerability of the heart to fibrillation.

Acknowledgments

This research was supported in part by awards from the Whitaker Foundation, NIH Grant HL47505, the Nora Eccles Treadwell Foundation, and the Richard A. and Nora Eccles Harrison Fund for Cardiovascular Research. The authors would like to thank B. Taccardi for the experimental data, and R.S. MacLeod and J.A. Schmidt for their valuable comments and suggestions.

References

- [1] M. A. Allesie, F. I. M. Bonke, and J. G. Schopman. Circus movement in rabbit atrial muscle as a mechanism of tachycardia III. The leading circle concept: A new model of circus movement in cardiac tissue without the involvement of an anatomical obstacle. *Circulation Research*, 4:9–18, 1977.
- [2] H. A. Fozzard, E. Haber, R. B. Jennings, A. M. Katz, and H. E. Morgan, editors. *The Heart and Cardiovascular System*, volume 2, chapter Janse M.J.:Reentry Rhythmus, pages 1203–1238. 1986.
- [3] M. A. Allesie, M. J. Schalij, C. J. H. L. Kirchoff, L. Boersma, M. Huybers, and J. Hollen. Experimental electrophysiology and arrhythmogenicity. Anisotropy and ventricular tachycardia. *European Heart Journal*, 10 (supplement E):2–8, 1989.
- [4] R.W. Joyner, R. Ramon, and J.W. Moore. Simulation of action potential propagation in an inhomogenous sheet of coupled excitable cells. *Circulation Research*, 36:654–661, 1975.
- [5] L.J. Leon and B. M. Horáček. Computer model of excitation and recovery in the anisotropic myocardium I. Rectangular and cubic arrays of excitable elements. *J. Electrocardiol*, 24:1–15, 1991.
- [6] L.J. Leon and B. M. Horáček. Computer model of excitation and recovery in the anisotropic myocardium II. Excitation in the simplified left ventricle. *J. Electrocardiol*, 24:17–31, 1991.
- [7] L.J. Leon and B. M. Horáček. Computer model of excitation and recovery in the anisotropic myocardium III. Arrhythmogenic conditions in the simplified left ventricle. *J. Electrocardiol*, 24:33–41, 1991.
- [8] L.J. Leon and F.A. Roberge. Structural complexity effects on transverse propagation in a two dimensional model of myocardium. *IEEE Trans. Biomed. Eng.*, 38(10):997–1009, Oct 1991.
- [9] L.J. Leon and F.A. Roberge. Directional characteristics of action potential propagation in cardiac muscle. A model study. *Circulation Research*, 69:378–395, 1991.
- [10] C.S. Henriquez and R. Plonsey. Simulation of propagation along a bundle of cardiac tissue. *IEEE Trans. Biomed. Eng.*, BME-37:850–860, 1990.
- [11] C.S. Henriquez and R. Plonsey. Results of simulation. *IEEE Trans. Biomed. Eng.*, BME-37:861–875, 1990.
- [12] B.J. Roth. Action potential propagation in a thick strand of cardiac muscle. *Circulation Research*, 68:162–173, 1991.

- [13] P. Colli Franzone, L. Guerri, and Taccardi B. Spread of excitation in a myocardial volume. simulation studies in a model of anisotropic ventricular muscle activated by point stimulation. *Journal of Cardiovascular Electrophysiology*, 4(2):144–160, April 1993.
- [14] P. Colli Franzone, Guerri L., and B. Taccardi. Potential distributions generated by point stimulation in a myocardial volume. stimulation studies in a model of anisotropic ventricular muscle. *Journal of Cardiovascular Electrophysiology*, 4(4):438–458, August 1993.
- [15] J.P. Keener. An eikonal–curvature equation for action potential propagation in myocardium. *Journal of Math. Biol.*, 29:629–651, 1991.
- [16] P Colli-Franzone, L. Guerri, and C. Viganotti *et al.* Potential fields generated by oblique dipole layers modeling excitation wavefronts in the anisotropic myocardium:Comparisons with potential fields elicited by paced dogs hearts in a volume conductor. *Circulation Research*, 52:706, 1982.
- [17] P. Colli Franzone, L. Guerri, and C. Viganotti. Oblique dipole layer potentials applied to electrocardiology. *Journal of Math. Biol.*, 17:93–114, 1983.
- [18] P. Colli Franzone, L. Guerri, and E. Magenes. Oblique dipole layer potentials for the direct and inverse problems of electrocardiology. *Math. Biosci.*, 68:23–55, 1984.
- [19] P. Colli Franzone, L. Guerri, and S. Rovida. Wavefront propagation in an activation model of the anisotropic cardiac tissue:Asymptotic analysis and numerical simulations. *Journal of Math. Biol.*, 28:121–176, 1990.
- [20] P. Colli Franzone, L. Guerri, and S. Tentoni. Mathematical modelling of the excitation process in the myocardial tissue:Influence of the fiber rotation on the wavefront propagation and the potential field. *Math. Biosci.*, pages 155–235, 1990.
- [21] G. K. Moe, W. C. Rheinboldt, and J. A. Abildskov. A computer model of fibrillation. *American Heart Journal*, 67:200–220, 1964.
- [22] N.V. Thakor and Eisenman L.N. Computer generation of fibrillation in a 3–Dimensional model of the heart. *Computers in Cardiology*, pages 391–394, 1988.
- [23] N.V. Thakor and Eisenman L.N. Three-dimensional computer model of the heart: Fibrillation induced by extrastimulation. *Computers and Biomedical Research*, 22:532–545, 1989.
- [24] Adam D. Propagation of depolarization and repolarization processes in the myocardium – An anisotropic model. *IEEE Trans. Biomed. Eng.*, BME-38:133–141, 1991.
- [25] R. Killman. *Three-Dimensional Numerical Simulation of the Excitation and Repolarization Process in the Entire Human Heart with Special Emphasis on Reentrant Tachycardias*. PhD thesis, Graz University of Technology, 1990.

- [26] D. Wei, O. Okazaki, K. Harumi, E. Harasawa, and H. Hosaka. Comparative simulation of excitation and body surface electrogram with isotropic and anisotropic computer heart models. *IEEE Trans. Biomed. Eng.*, 42(4):343–357, April 1995.
- [27] D. Adam. 3-Dimensional anisotropic model of myocardial electrical propagation. *Computers in Cardiology*, pages 405–408, 1985.
- [28] L.J. Leon and B. M. Horáček. Excitation in three-dimensional anisotropic cardiac tissue: A model study. *Proceedings of the IEEE*, pages 83–84, 1989.
- [29] P. M. F. Neilsen, I. J. LeGrice, B. H. Smail, and P. J. Hunter. A mathematical model of the geometry and fibrous structure of the heart. *American Journal of Physiology*, 260:H1365–H1378, 1991.
- [30] L. V. Corbin and A. M. Scher. The canine heart as an electrocardiographic generator. *Circulation Research*, 41:58–67, 1977.
- [31] J. A. Abildskov. Mechanism of the vulnerable period in a model of cardiac fibrillation. *Journal of Cardiovascular Electrophysiology*, 1:303–308, 1990.
- [32] J. A. Abildskov and R. L. Lux. The mechanism of simulated Torsade de Pointes in a computer model of propagated excitation. *Journal of Cardiovascular Electrophysiology*, 2:224–237, 1991.
- [33] J. A. Abildskov and R. L. Lux. Local events in a computer model of cardiac excitation. *Journal of Cardiovascular Electrophysiology*, 2:45–52, 1991.
- [34] M. J. Burgess, L. S. Green, K. Miller, R. Wyatt, and J.A. Abildskov. The sequence of normal ventricular recovery. *American Heart Journal*, 84:660–669, 1972.
- [35] P.B. Gharpure, H.W. Shen, and C.R. Johnson. Visualization of 3–D wave propagation in the heart – A new technique. *Proceedings of the IEEE EMBS 16th Annual International Conference*, 1994.
- [36] HanWei Shen and C.R. Johnson. Differential volume rendering:A fast algorithm for scalar field animation. *IEEE Visualization 94*, pages 188–195, 1994.
- [37] R. S. MacLeod, P. R. Ershler, C. R. Johnson, and M. A. Matheson. Map3d: Scientific visualization program for multichannel time series data on unstructured, three-dimensional meshes. Technical Report UUCS-94-016, Department of Computer Science, University of Utah, 1994.
- [38] M. Aoki, Y. Okamoto, T. Musha, and K.I. Harumi. Three-dimensional simulation of the ventricular depolarization and repolarization processes and body surface potentials:normal heart and bundle branch block. *IEEE Trans. Biomed. Eng.*, BME-34:519–531, 1987.
- [39] B Taccardi, R.L. Lux, P.R. Ershler, R.S. MacLeod, C Zabawa, and Y Vyhmeister. Potential distribution and excitation time maps recorded with high spatial resolution from the entire

ventricular surface of exposed dog hearts. *Proceedings of the Computers in Cardiology 1992, IEEE press*, Oct 1992.

- [40] G. Arisi, E. Macchi, C. Corradi, R. L. Lux, and B. Taccardi. Epicardial excitation during ventricular pacing, relative independence of breakthrough sites from the excitation sequence in canine right ventricle. *Circulation Research*, 71(4):840–849, October 1992.
- [41] P. B. Gharpure and C.R. Johnson. A 3–D cellular automata model of the heart. *IEEE Engineering in Medicine and Biology Society 15th Annual Interational Conference*, pages 752–753, 1993.

List of Figures

1	Model representations of fiber, sheet and cross sheet directions	5
2	A simulated action potential showing the different states 1–5	5
3	Activation shown propagating along the fastest available path	8
4	Graphical User Interface for Stimulus Sites and Dead Cells	9
5	Visualizing Activation in the Right and Left Ventricular Endocardia.	11
6	Isochrones from Site #2 under Isotropic conditions	15
7	Isochrones from Site #2	15
8	Isochrones from site #16	16
9	Isochrones from site #31	16
10	Isochrones from site #36	17
11	Isochrones from site #39	17
12	Isochrones from site #40	18
13	Isochrones from site #43	18
14	Isochrones from site #44	19
15	Isochrones from site #5	19
16	Isochrones from site #8	20